Nonlinear Dyn (2019) 97:733–748
https://doi.org/10.1007/s11071-019-05009-2

ORIGINAL PAPER

Bifurcation analysis on the effect of store-operated and receptor-operated calcium channels for calcium oscillations in astrocytes

Anqi Zhou · Xijun Liu · Pei Yu

Received: 3 December 2018 / Accepted: 9 May 2019 / Published online: 22 May 2019

Abstract Experimental evidence has proved that calcium ions (Ca^{2+}) play an important role in cellular physiological processes via calcium oscillations. The entry rate of Ca^{2+} into cells through plasma membrane cells is a major modulator of intracellular Ca^{2+} dynamics, including the voltage-gated Ca^{2+} channel, the store-operated Ca^{2+} channel (SOCC) and the receptor-operated Ca^{2+} channel (ROCC). In this paper, we modify an established four-dimensional dynamical model, which contains the SOCC and ROCC, and carry out a bifurcation analysis to study dynamics of the model. In particular, Hopf bifurcation is identified with the maximum flow of the SOCC chosen as the bifurcation parameter, and normal form theory is applied to consider the stability of bifurcating limit cycles. Bifurcation of multiple limit cycles arising from generalized Hopf bifurcation is also discussed, which may yield complex dynamical behaviors. Further, it is shown that the variation of the maximum flows for different calcium channels determines the parameter range for stable oscillations, as well as for the frequency and amplitude of oscillations. The results indicate that Hopf bifurcation is the main source to generate oscillating behaviors, yielding a different bistable phenomenon which involves stable limit cycle and stable equilibrium. Moreover, it is shown that partially blocking the SOCC or the ROCC can change the parameter region of stable calcium oscillations, and the ROCC has more impact than the SOCC on amplitude or frequency of calcium oscillations.

Keywords Calcium oscillation · Hopf bifurcation · Store-operated calcium channel · Receptor-operated calcium channel · Two-parameter bifurcation analysis

1 Introduction

Ca^{2+} signaling has been recognized as one of the most versatile second messengers in most cell types [1] which can cause complex dynamical behaviors [2], ranging from stochastic spiking to regular oscillations and from periodic waves to spiral waves. These Ca^{2+} oscillations and waves regulate an array of cellular functions as diverse as neuronal activity [3], cell apoptosis, gene transcription, muscle contraction [4], etc. Astrocyte, which is a type of glial cell, has been considered as a passive element of the brain. During the last decade, experiments indicate that astrocyte not only provides metabolic and structural support to the neuronal structures [5], but also plays an important role in communication processes with neuronal activity [6,7]. There exists bidirectional communication between astrocytes and neurons. Neuronal activity changes can increase astrocytic Ca^{2+}, while the vari-

A. Zhou · X. Liu
Department of Mechanics, Tianjin University, Tianjin 300354, China

P. Yu (✉)
Department of Applied Mathematics, Western University, London N6A 5B7, Canada
e-mail: pyu@uwo.ca

ation of Ca^{2+} can be fed back to the pre-synaptic and post-synaptic terminals and then evoke new responses in adjacent neurons [8]. Ca^{2+} oscillations and intercellular waves are generally observed in astrocytes after the Ca^{2+} waves were found within a cultured astrocytic syncytium in 1990s [9,10].

The entry rate of Ca^{2+} into cells is an important modulator of intracellular Ca^{2+} dynamics in all cell types. Therefore, Ca^{2+} channels play a key role in the initiation of the Ca^{2+} signal. There are four principal entry channels for Ca^{2+} influx, namely the voltage-gated channel (VGCC), the store-operated channel (SOCC), the receptor-operated channel (ROCC), and the ligand-gated channel (LGCC). The VGCC has significant influence on the excitable cells and muscle cells, while the SOCC and ROCC are the other two major calcium ions influx pathways, especially for non-excitable cells like astrocyte. The SOCC can be evoked when the intracellular store endoplasmic reticulum (ER) is depleted. Reports have shown that the store-operated Ca^{2+} entry (SOCE) is linked to several other Ca^{2+}-dependent processes, such as cell growth and death, regulation of enzyme activity [11] and the Alzheimer's disease [12]. In 2006, an attempt was made to establish a SOCC model in order to match experimental data [13]. However, the mechanisms of the SOCC are still not fully understood. The ROCC is open in the response agonist stimulation, independent of store depletion or depolarization and is used as the basis for the Ca^{2+} entry in most models. Results in [14] draw a closer analogy between the SOCC and ROCC.

In order to explore the underlying physiological mechanism of calcium oscillations, researchers have carried out lots of related experiments. Although a solid experimental foundation is necessary, mathematical modeling can also provide a significant approach to establish the inherent relation between the experimental data and parameters, which greatly save time and cost. Some models have been established for astrocytes and astrocytes-neuron networks over the past 15 years, which were developed for single astrocytes, see [15–17], while others were used to describe the interactions of astrocytes with neurons (eg., see [18–20]). Most of the models were developed on the basis of the two basic models established by Li and Rinzel [21] and Höfer et al. [22]. The cytosolic Ca^{2+} concentration used in [21] depends on the Ca^{2+}-induced Ca^{2+} release (CICR) mechanism under the assumption that the inositol triphosphate (IP_3) concentration maintains constant. However, the cytosolic Ca^{2+} concentration defined by Höfer et al. [22] depends not only on the CICR but also on the SERCA pump across the ER membrane mechanism, while the IP_3 concentration is varied via the two distinct production terms called PLCβ and PLCδ through phospholipase C (PLC). It has been observed that the fields of modeling the SOCC and ROCC are quite thin. The methods that many researchers have used to model the SOCC in astrocytes include the exhaustive approach [22], the phenomenological capture [18], and the one derived from experimental data [13]. The ROCC is often used as the basis for the Ca^{2+} entry and assumed to be an increasing algebraic function, or even a simple linear function of stimulation, which is usually described as the G protein activation [23] or the IP_3 production [24].

In this paper, we will modify a four-dimensional calcium oscillation model in astrocytes established by Riera et al. [25] in order to give a more sophisticated study. The original model contains the SOCC which, proposed by Di Garbo et al. [18], describes the SOCE effect. However, it has been found that the ROCC is also a major Ca^{2+} influx and is active by agonist stimulation or G protein. The ROCC influence on the amplitude and frequency of the Ca^{2+} concentration and the combined effect of the ROCC and SOCC on the Ca^{2+} oscillation are the main focus in research. Thus, in this paper we will include the ROCC in our mathematical model to give a more realistic analysis. In addition, a linear function for the IP_3 production is chosen to express the ROCC influence on the Ca^{2+} concentration in the cytosol. We will apply bifurcation theory to show the complex dynamical behavior of the model, including Hopf bifurcation from the positive equilibrium of the system. Further, normal form theory is applied to determine the stability of bifurcating limit cycles. We will also study bifurcation of multiple limit cycles and identify two limit cycles, showing bistable phenomenon. Two-parameter bifurcation graph is present to show the influence of different channel parameters on the amplitude and frequency of calcium oscillation in cytosol.

In the next section, we describe the modified four-dimensional calcium model. In Sect. 3, we use normal form theory to analyze Hopf bifurcation and determine the stability of bifurcating limit cycles. Moreover, multiple limit cycle bifurcation is studied and verified by simulation. In Sect. 4, the role of the SOCC and ROCC on calcium response is investigated by using

two-parameter bifurcation analysis. Finally, conclusion and discussion are drawn in Sect. 5.

2 Mathematical modeling

2.1 The original model

The original model, established and studied in [25], consists of four ordinary differential equations, which describe in detail the global Ca^{2+} signaling in astrocytes and estimate the remarkable parameters by a deductive reasoning strategy, showing a good consistency with experimental work. As shown in Fig. 1, this model contains one calcium store: the ER in cytosol. The Ca^{2+} concentration changes inside the ER occur through the activity of the IP_3R channel and the SERCA pump. So there are two flux channels in the ER: the V_{Rel} and the V_{SERCA}. The V_{Rel} represents the release from the ER to cytosol following the CICR mechanism, and V_{SERCA} denotes the Ca^{2+} uptake from cytosol to the ER. For the exchange from extracellular space, this model contains three fluxes: (i) the leakage Ca^{2+} influx, denoted as j_{in}; (ii) the extrusion across the plasma membrane, named V_{out}; and (iii) the influx of extracellular Ca^{2+} through the SOCC controlled by any unloading of the ER calcium store, called V_{SOCC}. These present main pathways of the Ca^{2+} in the original model. Thus, the model is described by the following equations for the exchange channels:

$$\begin{aligned} V_{Rel} &= c_1(v_1 m_\infty^3 h^3 + v_2)([Ca^{2+}]_{ER} \\ &\quad -[Ca^{2+}]_{Cyt}), \\ V_{SERCA} &= V_{SERCA}\frac{[Ca^{2+}]_{Cyt}^2}{k_{SERCA}^2 + [Ca^{2+}]_{Cyt}^2}, \\ V_{out} &= k_{out}[Ca^{2+}]_{Cyt}, \\ V_{SOCC} &= v_{SOCC}\frac{k_{SOCC}^2}{k_{SOCC}^2 + [Ca^{2+}]_{ER}^8}, \end{aligned} \tag{2.1}$$

where

$$\begin{aligned} m_\infty &= \frac{[IP_3]_{Cyt}[Ca^{2+}]_{Cyt}}{([IP_3]_{Cyt} + d_1)([Ca^{2+}]_{Cyt} + d_5)} \\ \left[Ca^{2+}\right]_{ER} &= \frac{[Ca^{2+}]_{free} - [Ca^{2+}]_{Cyt}}{c_1} \end{aligned} \tag{2.2}$$

There are four state variables involved in the model: the Ca^{2+} concentration in the cytosol, the total free Ca^{2+} concentration, the fraction of active IP_3R, and the IP_3 concentration. Consequently, the mathematical

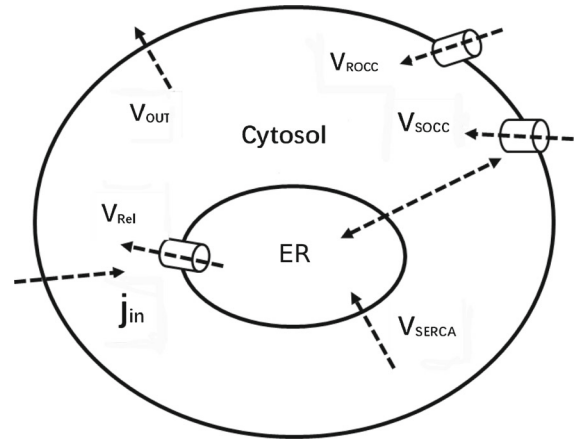

Fig. 1 Schematic presentation of the model (2.3)

model can be described by the following differential equations [25]:

$$\begin{aligned} \frac{d[Ca^{2+}]_{Cyt}}{dt} &= V_{Rel} - V_{SERCA} \\ &\quad + \varepsilon(j_{in} + V_{SOCC} - V_{out}), \\ \frac{d[Ca^{2+}]_{free}}{dt} &= \varepsilon(j_{in} + V_{SOCC} - V_{out}), \\ \frac{dh}{dt} &= \alpha_h(1-h) + \beta_h h, \\ \frac{d[IP_3]_{Cyt}}{dt} &= X_{IP_3} + V_{PLC} - k_{IP_3}[IP_3]_{Cyt}, \end{aligned} \tag{2.3}$$

where

$$\begin{aligned} \alpha_h &= a d_2 \frac{[IP_3]_{Cyt} + d_1}{[IP_3]_{Cyt} + d_3}, \\ \beta_h &= a[Ca^{2+}]_{Cyt}, \\ V_{PLC} &= v_\delta \frac{[Ca^{2+}]_{Cyt}^2}{[Ca^{2+}]_{Cyt}^2 + k_\delta^2}. \end{aligned} \tag{2.4}$$

Note in model (2.3) that except for the third variable, all other expressions are taken from [25], while that for the third variable is chosen from [26] since the authors of [26] found a typographical error in [25] for the third variable. The scaling factor $\varepsilon = A_{\rho m}/A_{ER}$ is introduced to emphasize that the surface of the plasma membrane $A_{\rho m}$ is much smaller than that of the ER membrane area A_{ER}. All the parameters in this model are positive, and the physical significance of the parameters is described in [25].

2.2 Our improved model

The receptor-operated calcium channel (ROCC) is another major Ca^{2+} influx pathway, which is open in direct response to agonist stimulation, independent of store depletion or depolarization. In recent years, the effect of the SOCC on the behavior of calcium ions has received much attention and a great deal has been learned about the molecular mechanisms underlying the SOCC [27,28]. However, it is believed that the connection between the SOCC and ROCC may be closely related. In this paper, we improve the model (2.3) by including the influence of the ROCC channel for the Ca^{2+} entry through the plasma membrane and the effect of the SOCC channel on the calcium ions. In most of existing models, the ROCC is usually used as the basis for the Ca^{2+} entry, so treated as a linear function. In this paper, we take the ROCC term used in [29], given by

$$J_{\mathrm{ROCC}} = v_{\mathrm{ROCC}}[\mathrm{IP_3}]_{\mathrm{Cyt}}. \tag{2.5}$$

It is seen from (2.5) that the IP_3 is a variable, implying that the neurotransmitters which activate the ROCC simultaneously liberate the IP_3. Meanwhile, these same neurotransmitters might also be expected to activate store-operated calcium entry as a result of IP_3-mediated depletion of ER. Moreover, the functional overlap between the two channel types may be identified. Thus, the improved model can be described by the following four-dimensional differential equations:

$$\begin{aligned}
\frac{\mathrm{d}y_1}{\mathrm{d}t} &= \frac{c_1 v_1 y_4^3 y_1^3 y_3 (\frac{y_2-y_1}{c_1} - y_1)}{(y_4+d_1)^3 (y_1+d_5)^3} \\
&\quad + c_1 v_2 \left(\frac{y_2 - y_1}{c_1} - y_1 \right) \\
&\quad - \frac{v_{\mathrm{SERCA}}\, y_1^2}{k_{\mathrm{SERCA}}^2 + y_1^2} + \varepsilon (j_{\mathrm{in}} + v_{\mathrm{ROCC}} y_4 \\
&\quad + \frac{v_{\mathrm{SOCC}} k_{\mathrm{SOCC}}}{k_{\mathrm{SOCC}}^2 + \frac{(y_2-y_1)^2}{c_1^2}} - k_{\mathrm{out}} y_1) \\
&\equiv f_1(y_1, y_2, y_3, y_4), \\
\frac{\mathrm{d}y_2}{\mathrm{d}t} &= \varepsilon (j_{\mathrm{in}} + v_{\mathrm{ROCC}} y_4 + \frac{v_{\mathrm{SOCC}} k_{\mathrm{SOCC}}}{k_{\mathrm{SOCC}}^2 + \frac{(y_2-y_1)^2}{c_1^2}} - k_{\mathrm{out}} y_1 \\
&\equiv f_2(y_1, y_2, y_4), \\
\frac{\mathrm{d}y_3}{\mathrm{d}t} &= \frac{a d_2 (y_4 + d_1)(1 - y_3)}{y_4 + d_3} - a y_1 y_3 \\
&\equiv f_3(y_1, y_3, y_4), \\
\frac{\mathrm{d}y_4}{\mathrm{d}t} &= X_{\mathrm{IP_3}} + v_\delta \frac{y_1^2}{y_1^2 + k_\delta^2} - k_{\mathrm{IP_3}} y_4 \\
&\equiv f_4(y_1, y_4),
\end{aligned} \tag{2.6}$$

where

$$y_1 = [\mathrm{Ca^{2+}}]_{\mathrm{Cyt}}, \; y_2 = [\mathrm{Ca^{2+}}]_{\mathrm{free}},$$
$$y_3 = h, \; y_4 = [\mathrm{IP_3}]_{\mathrm{Cyt}}$$

The typical parameter values are given in Table 1, among which except that for the V_{ROCC} chosen from [29], all are taken from [25]. As in this paper our particular interest is focused on the effect of the store-operated Ca^{2+} channel (SOCC) for the calcium oscillation, we thus choose the v_{SOCC} as the bifurcation parameter, denoted as α for convenience.

Table 1 Parameter values for model (2.6) [25,26]

Parameter	Value	Parameter	Value
a	0.2 μMs^{-1}	j_{in}	0.065 μMs^{-1}
c_1	0.185	v_1	6 s^{-1}
d_1	0.13 μM	v_2	0.11 s^{-1}
d_2	1.049 μM	$X_{\mathrm{IP_3}}$	0.3 μMs^{-1}
d_3	0.9434 μM	$k_{\mathrm{IP_3}}$	1.25 s^{-1}
d_5	0.082 μM	k_δ	0.55 μM
$v_{\mathrm{SOCC}}(\alpha)$	Bifurcation Parameter	ε	0.01
v_{ROCC}	0.2 μMs^{-1}	k_{SERCA}	0.1 μM
k_{out}	0.5 μMs^{-1}	k_{SOCC}	10 μM
v_{SERCA}	0.9 μMs^{-1}	v_δ	0.152 μMs^{-1}

3 Stability and bifurcation analysis

3.1 Equilibrium solutions

The equilibrium solutions of model (2.6), denoted as $E = (y_{10}, y_{20}, y_{30}, y_{40})$, can be obtained by setting $f_1(y_1, y_2, y_3, y_4) = f_2(y_1, y_2, y_4) = f_3(y_1, y_3, y_4) = f_4(y_1, y_4) = 0$. One may first solve $f_4 = 0$ to obtain y_{40}, then solve $f_3 = 0$ to find y_{30}. Next, solving $f_1 = 0$ yields y_{20}. Finally, substituting these solutions into $f_2 = 0$ one obtains a polynomial equation in y_{10} and α as follows:

$$F_1(y_{10},\alpha) = \frac{2}{3075} + \frac{59600\,y_{10}^2 + 11979}{82500000\,y_{10}^2 + 24956250} + \alpha\left\{\left[\frac{5832\,y_{10}\,f_{1a}}{25(2700\,(y_{10})^2+27)\,f_{2a}} - y_{10}^2\right]^2 + 100\right\}^{-1} - \frac{y_{10}}{200} = 0, \tag{3.1}$$

where f_{1a} and f_{2a} are polynomials in y_{10}, given by

$$\begin{aligned} f_{1a} = {} & 607466076524925341589831 68\,(y_{10})^{14} \\ & + 506344303607715860030658 9696\,(y_{10})^{23} \\ & + 698535415062701984706054 4716 \times 10^9\,(y_{10})^{12} \\ & + 835382163799260042755840 9766 \times 10^9\,(y_{10})^{11} \\ & + 607490100046232145016799 82889 \times 10^7\,(y_{10})^{10} \\ & + 428286730962488278849509 328687 \times 10^6\,(y_{10})^9 \\ & + 196270692755393040323994 866153736\,(y_{10})^{13} \\ & + 917041157613987782485124 476363392\,(y_{10})^{11} \\ & + 268544600480343615365746 768662549\,(y_{10})^{10} \\ & + 781395252272546783001403072 6966968\,(y_{10})^5 \\ & + 130265145681057747623207224 05487933\,(y_{10})^4 \\ & + 148335995035431853530705520 72565193\,(y_{10})^3 \\ & + 794682366575222855491953102 009945\,(y_{10})^2 \\ & + 180001354958020227297446089 67475\,y_{10} \\ & + 244540775586324168543781 03500, \end{aligned}$$

$$\begin{aligned} f_{2a} = {} & 151866519131231335397457 92 \times 10^9\,(y_{10})^{12} \\ & + 217464050244027874463514 624 \times 10^8\,(y_{10})^{11} \\ & + 243576571064909310495421 44 \times 10^9\,(y_{10})^{10} \\ & + 404772053973750667622597 69536 \times 10^6\,(y_{10})^9 \\ & + 127054470039628506760091 000448\,(y_{10})^8 \\ & + 189560123354275032984419 1314448\,(y_{10})^{11} \\ & + 280111271462053470817036 4893536\,(y_{10})^9 \\ & + 339924183822297821989941 240465\,(y_{10})^9 \\ & + 247435952439989440824560 916600240\,(y_{10})^4 \\ & + 211344108807164615066777 684574267\,(y_{10})^3 \\ & + 502518913093544238244978 2951705\,(y_{10})^2 \\ & + 279621340749030330437658 527025\,y_{10} \\ & + 611351938965810421359452 5875, \end{aligned}$$

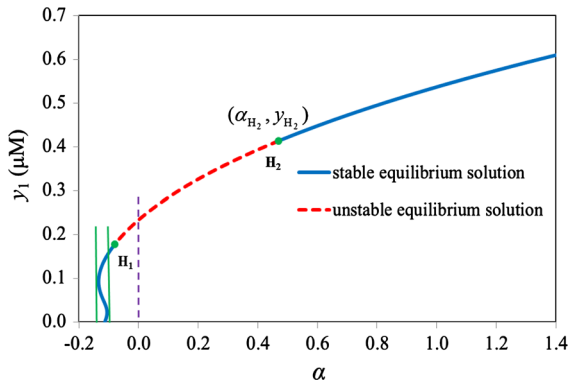

Fig. 2 Bifurcation diagram for system (2.6) projected on the α-y_1 plane, with the blue and red curves to denote stable and unstable equilibria, respectively. (Color figure online)

in which the parameter values given in Table 1 have been used. The bifurcation diagram is depicted in Fig. 2, showing the component y_1 of the equilibrium solution E with respect to α, i.e., $y_1 = y_{10}$ satisfying $F_1 = 0$. Note that the only biological meaningful part is for $\alpha > 0$. The vertical dotted line (in purple color) shown in Fig. 2 represents the equation $\alpha = 0$, implying that H_2 is the only biologically meaningful Hopf bifurcation point that we are interested.

3.2 Stability of the equilibrium E

In order to find the stability of the equilibrium E, we calculate the Jacobian of system (2.6) at E to get a fourth-degree characteristic polynomial,

$$P(\lambda,\alpha,y_{10}) = \lambda^4 + a_1(\alpha,y_{10})\lambda^3 + a_2(\alpha,y_{10})\lambda^2 + a_3(\alpha,y_{10})\lambda + a_4(\alpha,y_{10}). \tag{3.2}$$

According to Hurwitz Criterion [30], we know that the equilibrium E is asymptotically stable if all the roots of $P(\lambda,\alpha,y_{10})$ have negative real part, or equivalently, if all the Hurwitz arrangements $\Delta_i(\alpha,y_{10})$, $(i = 1,2,3,4)$ are positive, where

$$\begin{aligned} \Delta_1(\alpha,y_{10}) &= a_1(\alpha,y_{10}), \\ \Delta_2(\alpha,y_{10}) &= a_1(\alpha,y_{10})a_2(\alpha,y_{10}) - a_3(\alpha,y_{10}), \\ \Delta_3(\alpha,y_{10}) &= a_3(\alpha,y_{10})\Delta_2(\alpha,y_{10}) \\ &\quad - [a_1(\alpha,y_{10})]^2 a_4(\alpha,y_{10}), \\ \Delta_4(\alpha,y_{10}) &= a_4(\alpha,y_{10})\Delta_3(\alpha,y_{10}). \end{aligned} \tag{3.3}$$

When at least one of the Δ_i's becomes zero, the equilibrium E loses its stability and bifurcation occurs. In particular, saddle-node bifurcation happens at $a_4 = 0$ (and so $\Delta_4 = 0$), which yields single zero eigenvalue; and Hopf bifurcation may occur at $\Delta_3 = 0$, under which the characteristic polynomial P contains a pair of purely imaginary eigenvalues. In the following, we first investigate possible saddle-node bifurcation and then consider Hopf bifurcation.

To find whether a saddle-node bifurcation may occur, we need to determine the critical point at which P has a zero eigenvalue. To achieve this, we linearly solve α from $F_1 = 0$, i.e., $f_1 = 0$, to obtain a solution $\alpha = \alpha^*(y_{10})$ and then substitute the solution into a_4 and then solve $a_4 = 0$ to obtain two real solutions $y_{10} = 0.02160301$ and $y_{10} = 0.09255394$. Then, substituting these two solutions into $\alpha^*(y_{10})$ to get two values $\alpha^*_{s_1} = -0.10556702$ and $\alpha^*_{s_2} = -0.13382315$, respectively, which are shown in Fig. 2 as two green vertical lines. Therefore, due to $\alpha^*_{s_k} < 0, k = 1, 2$, there does not exist physically meaningful saddle-node bifurcation from the equilibrium E.

Next, we turn to consider possible Hopf bifurcations which may occur from the equilibrium E. We need the following theorem [31] to find the necessary and sufficient conditions under which Hopf bifurcation can occur.

Theorem 3.1 *The necessary and sufficient conditions for a Hopf bifurcation to occur from an equilibrium solution of the general dynamical system $\dot{x} = f(x)$, $x \in R^n$ are $\Delta_{n-1} = 0$, $a_n > 0$ and $\Delta_i > 0$ $(1 \le i \le n-2)$. where Δ_i are Hurwitz arrangements of the characteristic polynomial of the equilibrium solution.*

To examine whether a Hopf bifurcation may occur from the equilibrium E, we need to find the critical value of α at which the characteristic polynomial P contains a pair of purely imaginary eigenvalues (and other two eigenvalues still have negative real part). According to Theorem 3.1, the Hopf critical point is determined from $\Delta_3 = 0$. Similarly, we substitute $\alpha = \alpha^*(y_{10})$ into the equations $\Delta_3(\alpha, y_{10}) = 0$, and then solving this equation for y_{10}, together with the solution $\alpha^*(y_{10})$, yields two Hopf critical points: $(\alpha_{H_1}, y_{H_1}) = (-0.07995640, 0.17744973)$ and $(\alpha_{H_2}, y_{H_2}) = (0.46726717, 0.41318074)$. It is easy to see that only the solution (α_{H_2}, y_{H_2}) is biologically meaningful. These two Hopf critical points are shown in Fig. 2. At the critical point (α_{H_2}, y_{H_2}), other stability conditions given in Theorem 3.1 are satisfied:

$$\begin{aligned} &a_1 \approx 1.38541597, \quad a_2 \approx 0.18340547,\\ &a_3 \approx 0.25201194, \quad a_4 \approx 0.00027322,\\ &\Delta_2 \approx 0.00208093, \quad \Delta_3 \approx 9.012 \times 10^{-100} \approx 0, \end{aligned}$$

and the associated eigenvalues of system (2.6) evaluated at the equilibrium E are: $\pm 0.42622i$, -1.3843, and -0.00108.

Moreover, we need to verify the *transversality condition* of the Hopf bifurcation. Thus, suppose near the Hopf critical point, the characteristic polynomial P has a complex conjugate pair, given by

$$\beta(\alpha) \pm i\,\gamma(\alpha).$$

As we have obtained the solution $\alpha = \alpha^*(y_{10})$ from $F_1 = 0$, we may use the polynomials P and F_1, and apply inverse differentiation to obtain

$$\frac{\mathrm{d}\lambda}{\mathrm{d}\alpha} = \frac{\mathrm{d}\lambda}{\mathrm{d}y_{10}}\frac{\mathrm{d}y_{10}}{\mathrm{d}\alpha} = -\frac{\mathrm{d}\lambda}{\mathrm{d}y_{10}}\frac{\frac{\partial P}{\partial y_{10}}}{\frac{\partial P}{\partial \lambda}}\frac{1}{\frac{\mathrm{d}\alpha^*}{y_{10}}}.$$

Then, taking the real part and evaluating it at the Hopf critical point α_H, we obtain

$$\left.\frac{\mathrm{d}\beta}{\mathrm{d}\alpha}\right|_{\alpha=\alpha_H} = Re\left(\frac{\mathrm{d}\lambda}{\mathrm{d}\alpha}\right)\Big|_{\alpha=\alpha_H} \approx -0.189137 \neq 0,$$

which indeed indicates that Hopf bifurcation occurs at the critical point $\alpha = \alpha_H$.

3.3 Stability of limit cycles

Having identified the Hopf bifurcation point, from which a family of limit cycles (isolated periodic motion) are generated, we now ask how to know whether the bifurcating limit cycles are stable or not. Although a numerical simulation may indicate the stability of limit cycles, it does not provide analytical formulas to show how the stability of the limit cycles changes with respect to parameters. It is well known that for planar dynamical systems, the first Lyapunov constant, whose sign determines the stability of limit cycles, can be obtained using a simple formula based on the second and third derivatives of the vector field evaluated at the Hopf critical point. However, such closed-form formulas become much more involved and hard to calculate for higher-dimensional dynamical systems since it involves center manifold computation. So in

general, symbolic computations using a computer algebra system such as Maple are applied to find the Lyapunov constants. There exist many methods for computing the Lyapunov constants, one of which is the method of normal forms, which is an efficient computational approach for higher-dimensional systems and higher-order Lyapunov constants.

Now, we apply normal form theory and the Maple program developed in [32] to system (2.6) to analyze the Hopf bifurcation which occurs at the critical point (α_{H_2}, y_{H_2}). The normal form associated with a Hopf bifurcation, describing the dynamics on a two-dimensional center manifold near the critical point, can be written in polar coordinates as

$$\begin{aligned}\frac{\mathrm{d}r}{\mathrm{d}t} &= r(L_0\mu + L_1 r^2 + \cdots),\\ \frac{\mathrm{d}\theta}{\mathrm{d}t} &= \omega_c + \tau_0\mu + \tau_1 r^2 + \cdots\end{aligned}$$

where $\mu = \alpha - \alpha_{H_2}$. The coefficient L_1 is called the first Lyapunov constant or the first-order focus value, which determines the stability of bifurcating limit cycles. When $L_1 < 0$ (> 0), the Hopf bifurcation is called supercritical (subcritical), and the bifurcating limit cycles are stable (unstable).

Before applying the Maple program [32], we need to transfer the equilibrium to the origin and make the Jacobian of the system in Jordan canonical form. To achieve this, we introduce the transformation: $Y_1 = y_1 - 0.41318074$, $Y_2 = y_2 - 4.34589883$, $Y_3 = y_3 - 0.46143703$, $Y_4 = y_4 - 0.28372850$, and $\mu = \alpha - 0.46726717$ into system (2.6) and expand the resulting equations in Taylor series around the origin up to the third order. Further, introducing the following transformation:

$$\begin{bmatrix} y_1\\ y_2\\ y_3\\ y_4\end{bmatrix} = \begin{bmatrix} y_{10}(\mu)\\ y_{20}(y_{10},\mu)\\ y_{30}(y_{10},\mu)\\ y_{40}(y_{10},\mu)\end{bmatrix} + T\begin{bmatrix} Y_1\\ Y_2\\ Y_3\\ Y_4\end{bmatrix},$$

where

$$T = \begin{bmatrix} 4.9617492 & -3.3389010 & 0.1665505 & 0.7259937\\ 0.0334766 & 0.0519165 & 0.9956699 & 0.0037586\\ 0.2414924 & 1.0941556 & -0.0918431 & 0.0997996\\ 0.4632766 & -0.6098452 & 0.0225549 & -0.9140820\end{bmatrix}, \tag{3.4}$$

into (2.6) we obtain

$$\dot{Y}_i = F_i(Y_1, Y_2, Y_3, Y_4), \tag{3.5}$$

where $y_{10}(\mu)$ is determined from (3.1). Now, the Jacobian of system (3.5) evaluated at the origin, $Y_i = 0$, $i = 1, 2, 3, 4$, at the critical point, $\mu = 0$, is in the Jordan canonical form:

$$J|_{(0,0,0,0)} = \begin{bmatrix} 0 & \omega_c & 0 & 0\\ -\omega_c & 0 & 0 & 0\\ 0 & 0 & -0.0010850223 & 0\\ 0 & 0 & 0 & -1.38433095\end{bmatrix},$$

where $\omega_c = 0.42622679$. Applying the formulas given in [33] to system (3.5) yields the coefficients L_0 and τ_0.

$$\begin{aligned} L_0 &= \frac{1}{2}\left(\frac{\partial F_1}{\partial Y_1\partial\mu} + \frac{\partial F_2}{\partial Y_2\partial\mu}\right)|_{Y_i=0,\mu=0}\\ &= -0.189136908,\\ \tau_0 &= \frac{1}{2}\left(\frac{\partial F_1}{\partial Y_2\partial\mu} - \frac{\partial F_2}{\partial Y_1\partial\mu}\right)|_{Y_i=0,\mu=0}\\ &= 0.0056113642.\end{aligned} \tag{3.6}$$

Then, substituting $\mu = 0$ into system (3.5) and applying the Maple program [32] to the resulting system we obtain

$$L_1 = -11.98860783, \quad \tau_1 = -0.50752175.$$

Therefore, the normal form associated with the Hopf bifurcation up to the third order is given by

$$\begin{aligned}\frac{\mathrm{d}r}{\mathrm{d}t} &= r(L_0\mu + L_1 r^2 + \cdots)\\ &= r(-0.189136908\mu - 11.98860783r^2 + \cdots),\\ \frac{\mathrm{d}\theta}{\mathrm{d}t} &= \omega_c + \tau_0\mu + \tau_1 r^2 + \cdots\\ &= 0.42622679 + 0.00561136\mu\\ &\quad - 0.5075217r^2 + \cdots,\end{aligned} \tag{3.7}$$

It is clear that the Hopf bifurcation is supercritical since $L_1 < 0$. To verify the analytical predictions, we use model (2.6) to perform a simulation with the parameter values given in Table 1. For the supercritical Hopf bifurcation, when α decreases from $\alpha > \alpha_{H_2}$ to $\alpha < \alpha_{H_2}$ and passes through the critical point α_{H_2} (i.e., μ is varied to cross zero from positive to negative), the equilibrium loses its stability and bifurcates into stable limit cycles, as shown in Fig. 3a, b. When

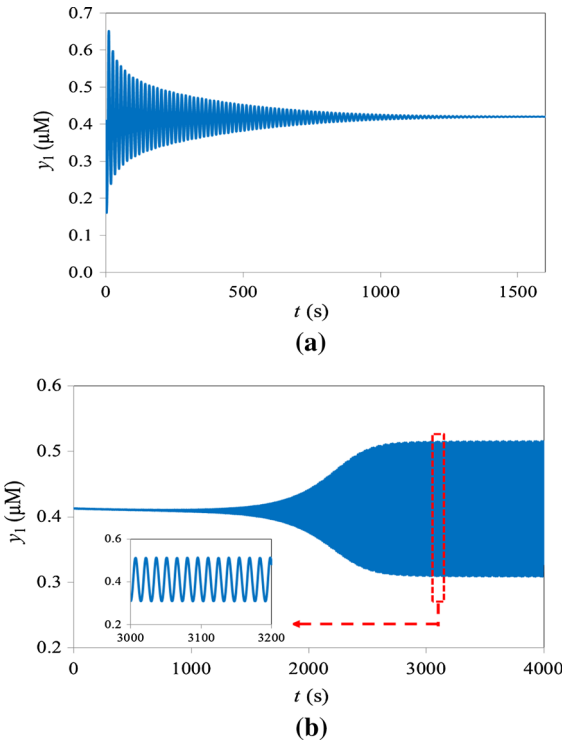

Fig. 3 Simulated time history for y_1 of system (2.6), **a** when $\alpha = 0.48\mu\text{Ms}^{-1}$, converging to the equilibrium E; and **b** when $\alpha = 0.45\mu\text{Ms}^{-1}$, converging to a stable limit cycle

$\alpha = 0.48 > \alpha_{H_2} = 0.46726717$, the solution trajectory converges to the stable equilibrium E, as shown in Fig. 3a, while when $\alpha = 0.45 < \alpha_{H_2} = 0.46726717$ the equilibrium becomes unstable and the trajectory converges to a stable limit cycle, see Fig. 3b.

3.4 Bifurcation of multiple limit cycles

Complex dynamics may arise from multiple limit cycle bifurcation. In this section, we will use normal form theory to prove the existence of two limit cycles bifurcating from the Hopf critical point (α_{H_2}, y_{H_2}). Firstly, we briefly introduce the method based on normal form theory. Suppose $\dot{\mathbf{x}} = T\mathbf{x} + \mathbf{f}(\mathbf{x})$ is a general nonlinear differential system, where $\mathbf{f}(\mathbf{x})$ represents the nonlinear part of the system and T is the Jacobian of the system. Moreover, suppose $\mathbf{x} = \mathbf{0}$ is an equilibrium point of the system and T contains a purely imaginary pair, and other eigenvalues have negative real parts. Then, by applying the normal form theory, we obtain the normal form given in polar coordinates as follows:

$$\begin{aligned} \dot{r} &= r(L_0 + L_1 r^2 + L_2 r^4 + \cdots + L_k r^{2k} + \cdots), \\ \dot{\theta} &= \omega_c + \tau_0 + \tau_1 r^2 + \tau_2 r^4 \cdots + \tau_k r^{2k} + \cdots, \end{aligned} \tag{3.8}$$

where r and θ represent the amplitude and phase of motion, respectively, and L_k and τ_k are expressed in terms of the original system's coefficients. L_0 and τ_0 are obtained from linear analysis, and L_k is called the kth Lyapunov constant or the kth-order focus value. The first equation of (3.8) can be used to investigate the bifurcation of limit cycles and their stability. To find k small-amplitude limit cycles of the system, we solve $L_0 = L_1 = \cdots = L_{k-1} = 0$, but $L_k \neq 0$. Then, appropriate small perturbations are performed to prove the existence of k limit cycles. The following theorem gives sufficient conditions for the existence of k small-amplitude limit cycles. (The proofs can be found in [34].)

Theorem 3.2 *Suppose the focus values of a dynamical system depend on k parameters, expressed as*

$$L_j = L_j(\epsilon_1, \epsilon_2, \ldots, \epsilon_k), \quad j = 0, 1, \ldots, k, \tag{3.9}$$

satisfying

$$\begin{aligned} &L_j(0, \ldots, 0) = 0, \ j = 0, 1, \ldots, k-1, \\ &L_k(0, \ldots, 0) \neq 0, \\ &\det\left[\frac{\partial(L_0, L_1, \ldots, L_{k-1})}{\partial(\epsilon_1, \epsilon_1, \ldots, \epsilon_k)}\right]_{(0,\ldots,0)} \neq 0. \end{aligned} \tag{3.10}$$

Then, for any given $\epsilon_0 > 0$, there exist $\epsilon_1, \epsilon_2, \ldots, \epsilon_k$ and $\delta > 0$ with $|\epsilon_j| < \epsilon_0$, j = 1, 2, ..., k such that the equation $\dot{r} = 0$ has exactly k real positive roots for r (i.e., the dynamical system has exactly k limit cycles) in a δ-ball with the center at the origin.

For the model (2.6), the IP_3 represents the stimulus intensity and is recognized as one of the most important agents for the depletion in the intercellular store ER, and the X_{IP_3} is considered as a basal level of cytosolic IP_3 production [25]. Hence, the X_{IP_3} plays an important role in the Ca^{2+} influx. So, in the following, in addition to α, the X_{IP_3} is chosen as a second bifurcation parameter, and the values of other parameters are chosen from Table 1. Denote the equilibrium solution of (2.6) as $E_G = (y_{1G}, y_{2G}, y_{3G}, y_{4G})$. Then, using a similar computation process as in Sect. 3.1, we

can get a polynomial equation $f_1(y_{1G}, \alpha, X_{IP_3}) = 0$. According to Theorem 3.1, the critical Hopf bifurcation point is determined by $\Delta_3(X_{IP_3}, \alpha, y_{1G}) = 0$. Therefore, $X_{IP_3} = G(\alpha, y_{1G})$ can be obtained from $\Delta_3(X_{IP_3}, \alpha, y_{1G}) = 0$ and then substituting $X_{IP_3} = G(\alpha, y_{1G})$ into $f_1(y_{1G}, \alpha, X_{IP_3})$ to get a function F_2 in y_{1G} and α. In the previous section, we have transferred the equilibrium E to the origin and make the Jacobian of the system (2.6) in Jordan canonical form. Now, the same process is applied to get the linear transformation T_G and the affine transformation,

$$\begin{bmatrix} y_1 \\ y_2 \\ y_3 \\ y_4 \end{bmatrix} = \begin{bmatrix} y_{1G} \\ y_{2G}(y_{1G}, \alpha) \\ y_{3G}(y_{1G}, \alpha) \\ y_{4G}(y_{1G}, \alpha) \end{bmatrix} + T_G \begin{bmatrix} Y_1 \\ Y_2 \\ Y_3 \\ Y_4 \end{bmatrix},$$

which are used to obtain the new system,

$$\dot{Y}_i = F_i(Y_1, Y_2, Y_3, Y_4, y_{1G}, \alpha). \tag{3.11}$$

Then, we apply the Maple program [32] for computing the normal form of system (3.11) to obtain L_1 and L_2 which are expressed in α and y_{1G}. Solving $L_1(\alpha, y_{1G}) = 0$ and $F_2(\alpha, y_{1G}) = 0$ for y_{1G} and α restricted to biologically meaningful values, we obtain $\alpha = 0.06298906$, y_{1G}=0.37747689. Then, $X_{IP_3} = G(\alpha, y_{1G}) = 0.56840217$. Thus, at the critical point defined by $\alpha = 0.06298906$, $X_{IP_3} = 0.56840217$, we have $L_1 = 0$ and $L_2 \approx -227.5876$. So by Theorem 3.2, we conclude that system (2.6) can have two small-amplitude limit cycles bifurcating from the equilibrium E_G due to Hopf bifurcation. To get the two small-amplitude limit cycles, we take small perturbations on X_{IP_3} and α as $X_{IP_3} = 0.56840217+\epsilon_1$, $\alpha = 0.06298906+\epsilon_2$, with $\epsilon_1 = 0.0001$ and $\epsilon_2 = 0.0000001$, for which the focus values become

$$L_0 \approx -6.89398415 \times 10^{-9}, \quad L_1 \approx 0.00329618,$$
$$L_2 \approx -92.94241575.$$

Thus, the truncated normal form equation $\dot{r} = L_0 + L_1 r^2 + L_2 r^4 = 0$ yields two positive roots: $r_1 \approx 0.0015$ and $r_2 \approx 0.0058$ which are the approximate amplitudes of the two limit cycles. Since $L_0 < 0$ and $L_2 < 0$, the equilibrium point $E_G = (0.37747689, 2.66095798, 0.54690561, 0.49353478)$ and the outer limit cycle are stable, while the inner limit cycle is unstable because $L_1 > 0$. In Fig. 4, two initial points: $(y_1, y_2, y_3, y_4) = (0.417056, 2.660542, 0.546936, 0.523611)$ and $(0.687056, 2.660542, 0.546936, 0.543611)$, are chosen to produce two trajectories. It is clear to see that the trajectory starting from the second initial point (in red color) converges to the outer stable limit cycle, and the trajectory starting from the first initial point (in blue color) also converges to the stable limit cycle, showing the existence of a stable limit cycle. The time history corresponding to the trajectory given in Fig. 4a is shown in Fig. 4b which demonstrates that both oscillations (in red and blue colors) converge to the stable limit cycle from two different initial conditions.

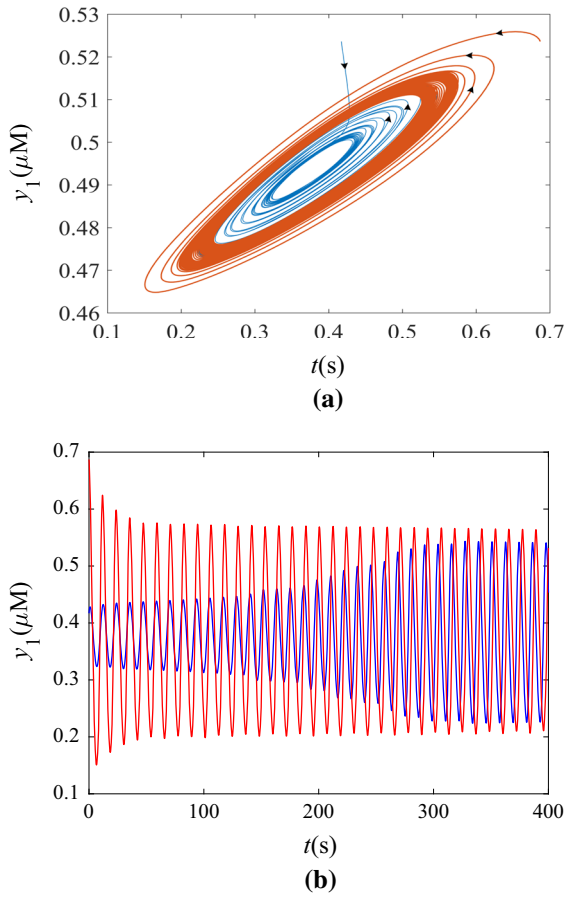

Fig. 4 Two simulated trajectories of system (2.6), converging to the same stable limit cycle, one from the initial points (y_1, y_2, y_3, y_4) = (0.417056, 2.660542, 0.546936,0.523611)(in red color) and the other from (y_1, y_2, y_3, y_4) = (0.687056, 2.660542, 0.546936, 0.543611)(in blue color): **a** phase portrait; and **b** time history. (Color figure online)

The above result shows an interesting new bistable phenomenon involving coexisting stable equilibrium and stable limit cycle, as depicted in Fig. 5a, where

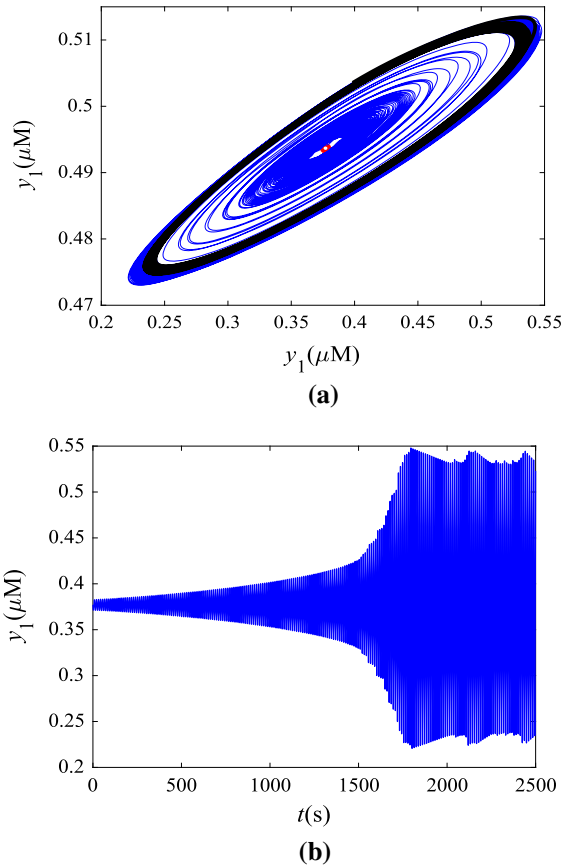

Fig. 5 Simulation of system (2.6), showing the bistable phenomenon with a stable equilibrium and a stable limit cycle: **a** phase diagram; and **b** time history

the red circle denotes the coexisting stable equilibrium, E_G, of the astrocyte cell, while the blue curve represents the coexisting stable calcium oscillation. Since the E_G is stable, there must exist an unstable limit cycle on an invariant manifold between the E_G and the stable limit cycle, which is a separatory dividing the whole phase plane into two trapping regions, one for the stable equilibrium and one for the stable limit cycle. The time history is displayed in Fig. 5b.

4 Numerical simulation of the calcium ions entry via SOCC and ROCC

4.1 The roles of store-operated calcium ions entry

The store-operated Ca^{2+} entry (SOCE) via the SOCC, also called capacitative Ca^{2+} entry(CCE), has been observed in many different cell types and recorded electro-physiologically as a persistent current. It is an influx of Ca^{2+} from the extracellular space that happens when intercellular Ca^{2+} stores are sufficiently depleted [35].

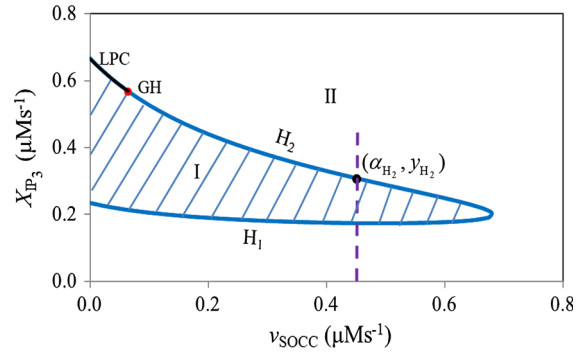

Fig. 6 The two-parameter bifurcation diagram in α and X_{IP_3}

4.1.1 Effect on the calcium response

The IP_3 is recognized as one of the most important agents for the depletion in the intercellular store ER, leading to the opening of plasma membrane Ca^{2+} channels. In our model, we consider the X_{IP_3} to be a basal level of cytosolic IP_3 production like the extrinsic IP_3 fluctuations. Therefore, in this section we use bifurcation analysis to investigate the interaction between the store-operated Ca^{2+} entry (SOCE) and the IP_3.

The two-parameter bifurcation diagram, as shown in Fig. 6, uses the X_{IP_3} and v_{SOCC} as bifurcation parameters. The region (I) (shaded area) represents the area where stable oscillations exist. The intersection point of the vertical dashed line and the curve (H_2) represents a Hopf critical point (α_{H_2}, y_{H_2}), which is the same as that shown in Fig. 2. The generalized Hopf critical point is denoted by GH, at which the first Lyapunov constant $L_1 = 0$, leading to bifurcation of multiple limit cycles, as discussed in Sect. 3.4, where the fold bifurcation of limit cycles, labeled by LPC, is the curve in black color. As shown in Fig. 6, with the v_{SOCC} decreasing, the corresponding value of X_{IP_3} for the first Hopf bifurcation point (H_1) shows a slight change while the corresponding value of X_{IP_3} for the second Hopf bifurcation point (H_2) displays a gradual increase. Due to the change in the second bifurcation point, the interval of the X_{IP_3} in the shaded area (a vertical line segment) increases as the v_{SOCC} decreases, implying that as the maximal rate

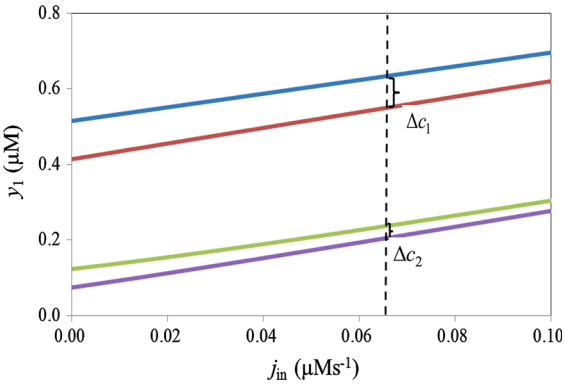

Fig. 7 Impact on cytosol due to the change in basal Ca^{2+} levels with respect to j_{in} with the values of the SOCC chosen from region II in Fig. 4a. v_{SOCC} = 0.1 μMs^{-1}, X_{IP_3} = 1.2 μMs^{-1} (blue line), v_{SOCC} = 0.01 μMs^{-1}, X_{IP_3} = 1.2 μMs^{-1} (red line), v_{SOCC} = 0.1 μMs^{-1}, X_{IP_3} = 0.2 μMs^{-1} (green line), v_{SOCC} = 0.01 μMs^{-1}, X_{IP_3} = 0.2 μMs^{-1} (purple line). (Color figure online)

of the SOCC influx decreases, the stimulus intensity which causes the Ca^{2+} in cytosol to oscillate increases slightly, while higher stimulus intensity is required in order for the system to return to the resting state as the maximal rate of the SOCC influx decreases. Moreover, as the v_{SOCC} goes to zero, the value of X_{IP_3} is still meaningful and realistic. So with zero SOCE flux, the sustained oscillations still exist, and so adequately blocking the v_{SOCC} may increase the region of stable calcium oscillations.

Figure 6 mainly shows the effects of the v_{SOCC} and X_{IP_3} on Hopf bifurcation. When the value of the v_{SOCC} and X_{IP_3} is chosen from region II, the trend of basal Ca^{2+} concentration cytoplasm as the v_{SOCC} and X_{IP_3} are varied is shown in Fig. 7. Two estimated values of the SOCE influx with maximal rate v_{SOCC} are chosen for the Ca^{2+} concentration: 0.01 μMs^{-1} and 0.1 μMs^{-1}. Moreover, a smaller value 0.2 μMs^{-1} and a larger value 1.2 μMs^{-1} are chosen for the IP_3 production rate X_{IP_3} to reflect two contrasting situations. It is seen from Fig. 7 that four lines are almost parallel, implying that the X_{IP_3} and v_{SOCC} have no or little influence on the growth rate of the basal Ca^{2+} in cytoplasm. In model (2.6), j_{in} is taken as 0.065 μMs^{-1} which is depicted by the dotted line in Fig. 7. Also, it is observed from this figure that for the smaller value of X_{IP_3} (shown in green and purple lines), the increment Δc_2 is small, indicating that the v_{SOCC} does not have an obvious impact on the change in the basal Ca^{2+} level. For the larger value of X_{IP_3} (shown in red and blue lines), the change in the basal Ca^{2+} level Δc_1 is larger than Δc_2, implying that the v_{SOCC} has a more remarkable effect under this condition. For a fixed value of v_{SOCC} (comparing the blue line with the green line or the red line with the purple line), a larger value of X_{IP_3} yields an obvious larger value of Ca^{2+} concentration in cytosol, which implies that higher stimulus intensity in X_{IP_3} forces the calcium store ER to release Ca^{2+} from the ER into cytosol and a decrease in the Ca^{2+} concentration in the ER can cause the Ca^{2+} to flow from extracellular into intercellular via the SOCC, yielding higher Ca^{2+} concentration in cytosol.

4.1.2 Simulation of the calcium flux for blocking or opening the SOCC

Experiments have manifested that the flux through the SOCC can be activated when the ER is depleted [36]. Using our model (2.6), we can simulate the calcium flux by blocking or opening the SOCC and SERCA with the parameter values close to the experimental data [37] as shown in Fig. 8, where four phases are indicated. The phase I corresponds to a steady state at the beginning, and then, the removal of calcium ions from the extracellular space can be simulated by setting $j_{in} = v_{SOCC} = 0$ at $t = 2000s$. A gradual decrease in the Ca^{2+} in cytosol is observed since the flux goes into the extracellular space (phase II). Then, the SERCA pump is set to zero at $t = 6000s$, causing a calcium spike in cytosol (phase III). This is because blocking the SERCA channel results in a one-way flow from ER into cytosol. As the Ca^{2+} concentration in cytosol gets higher, the calcium ions can be removed from the cytosol to extracellular space via V_{out} pump. At $t = 10000s$, the calcium is reintroduced into the extracellular space by setting $v_{SOCC} = 0.01$ and calcium ions rapidly reenter cells (phase IV).

4.1.3 Effect on the frequency and amplitude of calcium oscillation

Various types of complex physiological information in cells can be transmitted via oscillating waves, occurring by means of the frequency modulation (FM) and amplitude modulation (AM). Therefore, the frequency or amplitude is crucial in regulating mechanisms [38]. In this section, we investigate how the v_{SOCC} affects the changes in frequency, amplitude, and the range of stable oscillations. Figure 9a, b shows the changes in the

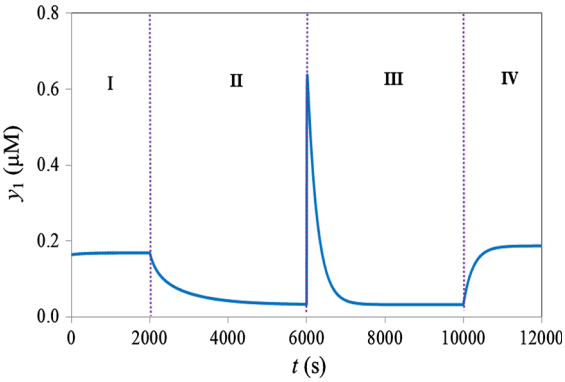

Fig. 8 Simulation of blocking (SOCC and SERCA)

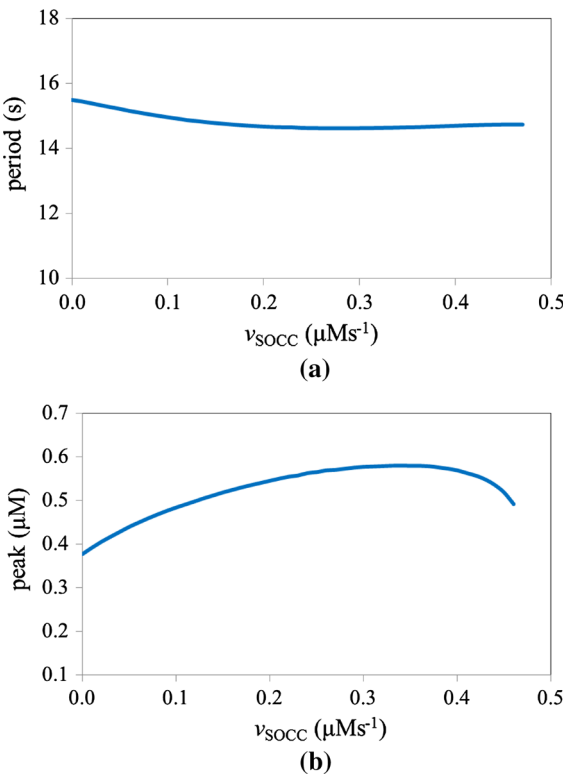

Fig. 9 **a** Change in the period of calcium oscillation versus v_{SOCC} (X_{IP_3} = 0.3); and **b** change in the amplitude of calcium oscillation versus v_{SOCC} (X_{IP_3} = 0.3)

period and amplitude of the calcium oscillation as the v_{SOCC} is varied with the fixed $X_{IP_3} = 0.3$ μMs^{-1}. It is seen from Fig. 9a that as the value of v_{SOCC} gets bigger, the period of the calcium oscillation changes slightly, which demonstrates that v_{SOCC} has little impact on the frequency of the calcium oscillation. However, as shown in Fig. 9b, the amplitude of the calcium oscillation first has a gradual increase and then decreases as the v_{SOCC} gets bigger. These observations indicate that the Ca^{2+} concentration in cytosol does not always grow as the v_{SOCC} increases, and may depend on the Ca^{2+} concentration in the intercellular Ca^{2+} store ER during the calcium oscillation.

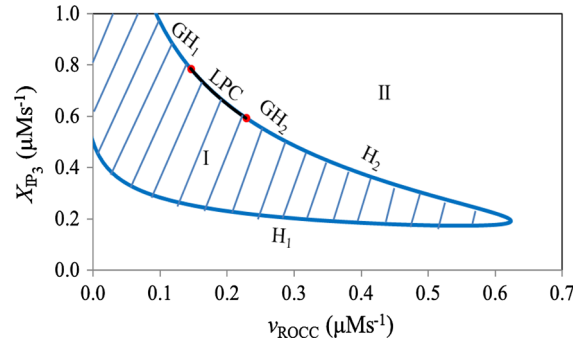

Fig. 10 The two-parameter (V_{ROCC}, X_{IP_3})bifurcation diagram

4.2 The roles of the receptor-operated calcium ions entry

4.2.1 Effect on the calcium response

Receptor-operated Ca^{2+} channels open in direct response to agonist stimulation. It has been mentioned that the IP_3 represents the stimulus intensity and the X_{IP_3} is considered as a basal level of the cytosolic IP_3 production. Hence, a two-parameter bifurcation diagram is more appropriate to display the dynamical behaviors as shown in Fig. 10, where the v_{ROCC} and X_{IP_3} are treated as bifurcation parameters. It can be seen that there exist two generalized Hopf critical points (GH_1, GH_2) at which the first focus value vanishes. The black curve labeled LPC is the fold bifurcation of the limit cycle, which connects the two generalized Hopf critical points and exhibits two limit cycles. As the v_{ROCC} decreases, the corresponding value of X_{IP_3} for the first Hopf bifurcation point (H_1) shows a slight change first and then becomes sharp, while that for the second Hopf bifurcation point (H_2) displays a gradual increase, causing the width of the oscillatory interval (the length between H_1 and H_2 on a same vertical line) to increase as the v_{ROCC} decreases. The oscillation can be avoided by decreasing the X_{IP_3} to 0.1, yielding a sufficient distance away from the oscillatory area (the shaded region), indicating that reasonable stimulus

intensity can control the oscillatory regime appropriately. However, partially blocking the v_{ROCC} influx can create a larger oscillatory regime and the system may oscillate even when the v_{ROCC} is completely blocked provided that the stimulus intensity is strong enough.

4.2.2 *Effect on the frequency and amplitude of the calcium oscillation*

How the v_{ROCC} affects the frequency and amplitude of the calcium oscillation in cytosol is shown in Fig. 11 for a wide range of the X_{IP_3} values. Four estimated values are chosen for the v_{ROCC}: 0.05 μMs^{-1}, 0.1μMs^{-1}, 0.2μMs^{-1} and 0.4μMs^{-1}. It can be seen that for a wide range of the X_{IP_3} values, larger values of the v_{ROCC} cause the period of oscillation to have a sharper decent rate with a narrowed oscillatory region according to Fig. 11a. The maximal period of the calcium oscillation increases as the v_{ROCC} grows, as shown in the same figure. Moreover, it is seen from Fig. 11a that for fixed values of X_{IP_3} (indicated by the vertical dotted line), the period of oscillation increases as the v_{ROCC} decreases. On the other hand, as shown in Fig. 11b, the amplitude peak of the calcium oscillation decreases as the v_{ROCC} decreases for a fixed value of X_{IP_3} (along the vertical dotted line). For a range of X_{IP_3} values, larger values of v_{ROCC} cause the amplitude peak to have a sharper ascent rate. These results imply that using the IP_3 as a stimulation may be efficient in controlling the frequency and amplitude of calcium oscillation. When an external stimulus arrives at the cell surface, a series of calcium spikes is activated. Then, cells may encode the information by varying the frequency and amplitude of the oscillation. Further, variation of the v_{ROCC} can increase cytoplasmic calcium ions directly, which may activate a process of calcium-induced calcium release (CICR). Any process that influences the CICR may change the refilling period of the calcium oscillation, and thus may alter the frequency and amplitude of the oscillation. The above findings are consistent with those reported in [39].

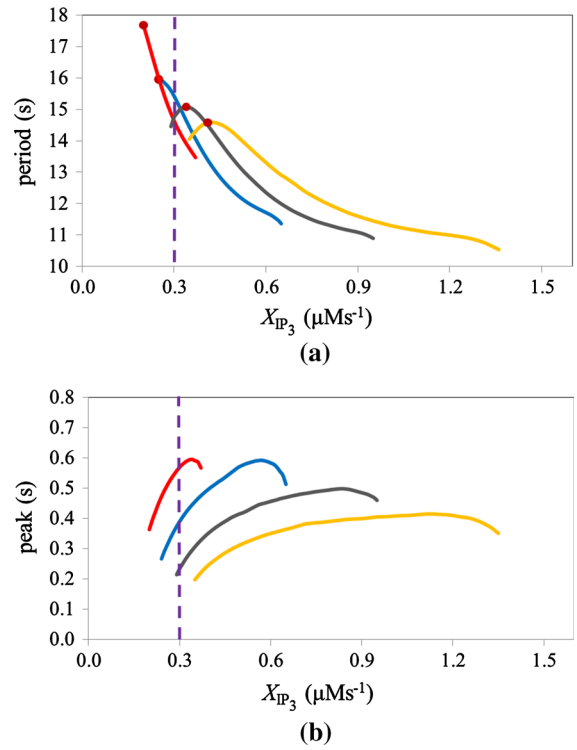

Fig. 11 **a** Period of the calcium oscillation versus X_{IP_3}; and **b** amplitude of the calcium oscillation versus X_{IP_3}, for various v_{ROCC} values: 0.4 μMs^{-1}(the red line), 0.2 μMs^{-1}(the blue line), 0.1 μMs^{-1}(the gray line), and 0.05 μMs^{-1}(the yellow line). (Color figure online)

5 Conclusion and discussion

In this paper, a four-dimensional calcium oscillation model is studied in detail, particularly for stability and bifurcation. The main goal is to study the effect of the SOCC and ROCC on the dynamical oscillating behavior and mutual interaction by using bifurcation and normal form theory.

We have modified an established four-dimensional model with the ROCC term, and chosen the maximal influx of the SOCC as a bifurcation parameter. Two Hopf critical points are identified by linear analysis, and the stability of limit cycles is obtained by employing the nonlinear analysis with the aid of normal form theory. The study shows that Hopf bifurcation is the source of oscillation behavior. We also investigate the bifurcation of multiple limit cycles, which may generate complex dynamical behaviors in biological systems. With the maximal influx of the SOCC and X_{IP_3} chosen as bifurcation parameters, we have shown that the four-dimensional model of the calcium oscillation can have two limit cycles due to generalized Hopf bifurcation, one of which is stable and the other is unstable, yielding a new bistable phenomenon consisting of a stable limit cycle (outer) and a stable equilibrium. In biological systems, equilibria and limit cycles are

two significant steady states for signal transduction. The coexistence of an stable equilibrium and a stable limit cycle may yield transform between these states, showing complex, yet more realistic dynamical behaviors. For example, codimension-2 bifurcations with bistable phenomenon in neuron have been investigated to achieve an important finding: Negative feedback can play a positive role in nonlinear dynamics (e.g., see [40]). Moreover, biological experiments have been performed on several types of cells to display bifurcations [41,42]. It is also noted that the above-discussed bifurcation scenarios with complex processes simulated in mathematical models match very well with those observed in experiments [3].

Moreover, the effects of the SOCC and the ROCC for the calcium amplitude and frequency are investigated. A two-parameter bifurcation diagram is present to show the relationship between the v_{SOCC} and $X_{\mathrm{IP_3}}$ for the Hopf bifurcation. The following results for the SOCC are obtained.

1. As the v_{SOCC} goes to zero, the $X_{\mathrm{IP_3}}$ is still biologically meaningful and realistic, implying that with zero SOCE flux, the sustained oscillations still exist, and so adequately blocking the SOCC will have a larger region for generating stable calcium oscillation.
2. For resting state of Ca^{2+}, larger $X_{\mathrm{IP_3}}$ causes an obvious higher Ca^{2+} concentration in cytosol for a same given value of v_{SOCC}. This shows that a higher stimulus intensity forces the calcium store ER to release Ca^{2+} from ER to cytosol and a decrease in the Ca^{2+} concentration in ER results in the Ca^{2+} inflow from extracellular.
3. The change in the amplitude of calcium oscillation first shows a gradual increase and then a decrease as the v_{SOCC} is increasing. The period of the calcium oscillation has almost no change, implying that the v_{SOCC} has little impact on the frequency of the calcium oscillation.

The results obtained for the ROCC are summarized below.

(a) Partially blocking the v_{ROCC} influx can yield a larger oscillatory regime, and the system can get into oscillation even when the v_{ROCC} is completely blocked as long as the stimulus intensity is strong enough. Thus, one can apply appropriate stimulus intensity to control the oscillatory regime as one wishes.

(b) Larger values of v_{ROCC} cause the period of calcium oscillation to have sharper decent rate, while the period increases as the v_{ROCC} decreases for a fixed $X_{\mathrm{IP_3}}$ value. The amplitude of the calcium oscillation decreases as the v_{ROCC} is decreased for a fixed $X_{\mathrm{IP_3}}$ value, while larger v_{ROCC} values may cause the amplitude to have a sharper ascent rate for a range of $X_{\mathrm{IP_3}}$ values. These results suggest that the IP_3 may be used to effectively control the frequency and amplitude of the calcium oscillation, and the v_{ROCC} may be used to change the period and amplitude of calcium oscillation by CICR mechanism.

Overall, the investigation on the SOCC and the ROCC shows that influxes from extracellular space into cytosol have an important influence on the formation and characteristics of the calcium oscillation in cytosol. Moreover, the SOCC and ROCC have coupling effect and the interaction between different Ca^{2+} influxes can also affect the dynamical properties such as the frequency and amplitude of the calcium oscillation in cytosol.

The study given in this paper reveals that the SOCC and ROCC are two critical channels in determining the dynamical behaviors of the calcium oscillation in astrocyte. The multiple limit cycle bifurcation occurring in the calcium oscillation model may be one of the sources to generate complex dynamics, which may explain some realistic complex dynamical phenomenon. Moreover, this method can be used to consider other nonlinear systems. Since the exact mechanism of the communication between the channels and intracellular calcium store is still under investigation, the simple model studied in this paper provides a good try to reach a good understanding. The systems used to modeling channels need to be updated as more experimental data become available. Meanwhile, as the complex feedback mechanisms are responsible for regulating intracellular calcium, the function of calcium oscillation is still unknown and needs a further study. Therefore, the actual roles in these channels require further evaluation and we hope that the results obtained in this paper are helpful in providing a theoretical basis for future research.

Acknowledgements This work is partially supported by the Natural Sciences and Engineering Research Council of Canada (No. R2686A02). A. Zhou also thanks the supports received from the Tianjin University Ph.D. Training Program and Western University.

References

1. Clapham, D.E.: Calcium signaling. Cell **80**(2), 259–268 (1995)
2. Ji, Q., Zhou, Y., Yang, Z., Meng, X.: Evaluation of bifurcation phenomena in a modified Shenčlarter model for intracellular Ca^{2+} bursting oscillations. Nonlinear Dyn. **84**(3), 1–8 (2016)
3. Gu, H., Pan, B.: A four-dimensional neuronal model to describe the complex nonlinear dynamics observed in the firing patterns of a sciatic nerve chronic constriction injury model. Nonlinear Dyn. **81**(4), 2107–2126 (2015)
4. Pinto, M.C., Tonelli, F.M., Vieira, A.L., Kihara, A.H., Ulrich, H., Resende, R.R.: Studying complex system: calcium oscillations as attractor of cell differentiation. Integr. Biol. **8**(2), 130–148 (2016)
5. Agulhon, C., Petravicz, J., McMullen, A.B., Sweger, E.J., Minton, S.K., Taves, S.R., Casper, K.B., Fiacco, T.A., McCarthy, K.D.: What is the role of astrocyte calcium in neurophysiology? Neuron **59**(6), 932–946 (2008)
6. Pellerin, L., Magistretti, P.J.: Neuroenergetics: calling upon astrocytes to satisfy hungry neurons. Neuroscientist **10**(1), 53–62 (2004)
7. Fellin, T., Pascual, O., Haydon, P.G.: Astrocytes coordinate synaptic networks: balanced excitation and inhibition. Physiology **21**(3), 208–215 (2006)
8. Navarrete, M., Perea, G., Maglio, L., Pastor, J., García de Sola, R., Araque, A.: Astrocyte calcium signal and gliotransmission in human brain tissue. Cereb. Cortex **23**(5), 1240–1246 (2012)
9. Cornell-Bell, A.H., Finkbeiner, S.M., Cooper, M.S., Smith, S.J.: Glutamate induces calcium waves in cultured astrocytes: long-range glial signaling. Science **247**(4941), 470–473 (1990)
10. Hamilton, N.B., Attwell, D.: Do astrocytes really exocytose neurotransmitters? Nat. Rev. Neurosci. **11**(4), 227 (2010)
11. Parekh, A.B., Putney Jr., J.W.: Store-operated calcium channels. Physiol. Rev. **85**(2), 757–810 (2005)
12. Putney Jr., J.W.: Presenilins, Alzheimer's disease, and capacitative calcium entry. Neuron **27**(3), 411–412 (2000)
13. Ong, H.L., Liu, X., Tsaneva-Atanasova, K., Singh, B.B., Bandyopadhyay, B.C., Swaim, W.D., Russell, J.T., Hegde, R.S., Sherman, A., Ambudkar, I.S.: Relocalization of STIM1 for activation of store-operated Ca^{2+} entry is determined by the depletion of subplasma membrane endoplasmic reticulum Ca^{2+} store. J. Biol. Chem. **282**(16), 12176–12185 (2007)
14. Shuttleworth, T.J.: Stim and orai proteins and the non-capacitative ARC channels. Front. Biosci. **17**, 847 (2012)
15. Ullah, G., Jung, P., Cornell-Bell, A.H.: Anti-phase calcium oscillations in astrocytes via inositol (1,4,5)-trisphosphate regeneration. Cell Calcium **39**(3), 197–208 (2006)
16. Lopez-Caamal, F., Oyarzún, D.A., Middleton, R.H., García, M.R.: Spatial quantification of cytosolic Ca^{2+} accumulation in nonexcitable cells: an analytical study. IEEE/ACM Trans. Comput. Biol. Bioinf. (TCBB) **11**(3), 592–603 (2014)
17. Riera, J., Hatanaka, R., Uchida, T., Ozaki, T., Kawashima, R.: Quantifying the uncertainty of spontaneous Ca^{2+} oscillations in astrocytes: particulars of Alzheimer's disease. Biophys. J. **101**(3), 554–564 (2011)
18. Di Garbo, A., Barbi, M., Chillemi, S., Alloisio, S., Nobile, M.: Calcium signalling in astrocytes and modulation of neural activity. Biosystems **89**(1–3), 74–83 (2007)
19. Dupont, G., Lokenye, E.F.L., Challiss, R.J.: A model for Ca^{2+} oscillations stimulated by the type 5 metabotropic glutamate receptor: an unusual mechanism based on repetitive, reversible phosphorylation of the receptor. Biochimie **93**(12), 2132–2138 (2011)
20. Postnov, D., Koreshkov, R., Brazhe, N., Brazhe, A., Sosnovtseva, O.: Dynamical patterns of calcium signaling in a functional model of neuron-astrocyte networks. J. Biol. Phys. **35**(4), 425–445 (2009)
21. Li, Y.X., Rinzel, J.: Equations for $InsP_3$ receptor-mediated Ca^{2+} oscillations derived from a detailed kinetic model: a hodgkin-huxley like formalism. J. Theor. Biol. **166**(4), 461–473 (1994)
22. Höfer, T., Venance, L., Giaume, C.: Control and plasticity of intercellular calcium waves in astrocytes: a modeling approach. J. Neurosci. **22**(12), 4850–4859 (2002)
23. Kummer, U., Olsen, L.F., Dixon, C.J., Green, A.K., Bornberg-Bauer, E., Baier, G.: Switching from simple to complex oscillations in calcium signaling. Biophys. J. **79**(3), 1188–1195 (2000)
24. Dupont, G., Goldbeter, A.: One-pool model for Ca^{2+} oscillations involving Ca^{2+} and inositol 1,4,5-trisphosphate as co-agonists for Ca^{2+} release. Cell Calcium **14**(4), 311–322 (1993)
25. Riera, J., Hatanaka, R., Ozaki, T., Kawashima, R.: Modeling the spontaneous Ca^{2+} oscillations in astrocytes: inconsistencies and usefulness. J. Integr. Neurosci. **10**(04), 439–473 (2011)
26. Manninen, T., Havela, R., Linne, M.L.: Reproducibility and comparability of computational models for astrocyte calcium excitability. Front. Neuroinform. **11**, 11 (2017)
27. Smyth, J.T., Hwang, S.Y., Tomita, T., DeHaven, W.I., Mercer, J.C., Putney, J.W.: Activation and regulation of store-operated calcium entry. J. Cell. Mol. Med. **14**(10), 2337–2349 (2010)
28. Soboloff, J., Rothberg, B.S., Madesh, M., Gill, D.L.: Stim proteins: dynamic calcium signal transducers. Nat. Rev. Mol. Cell Biol. **13**(9), 549 (2012)
29. Cao, P., Tan, X., Donovan, G., Sanderson, M.J., Sneyd, J.: A deterministic model predicts the properties of stochastic calcium oscillations in airway smooth muscle cells. PLoS Comput. Biol. **10**(8), e1003783 (2014)
30. Hinrichsen, D., Pritchard, A.J.: Mathematical Systems Theory I: Modelling, State Space Analysis, Stability and Robustness, vol. 48. Springer, Berlin (2005)
31. Yu, P.: Closed-form conditions of bifurcation points for general differential equations. Int. J. Bifurc. Chaos **15**(04), 1467–1483 (2005)
32. Yu, P.: Computation of normal forms via a perturbation technique. J. Sound Vib. **211**(1), 19–38 (1998)
33. Zhang, W., Yu, P.: Hopf and generalized hopf bifurcations in a recurrent autoimmune disease model. Int. J. Bifurc. Chaos **26**(05), 1650079 (2016)
34. Yu, P., Han, M.: Small limit cycles bifurcating from fine focus points in cubic order Z2-equivariant vector fields. Chaos Solitons Fractals **24**(1), 329–348 (2005)

35. Putney, J.W., Broad, L.M., Braun, F.J., Lievremont, J.P., Bird, G.S.J.: Mechanisms of capacitative calcium entry. J. Cell Sci. **114**(12), 2223–2229 (2001)
36. Malarkey, E.B., Ni, Y., Parpura, V.: Ca^{2+} entry through TRPC channels contributes to intracellular Ca^{2+} dynamics and consequent glutamate release from rat astrocytes. Glia **56**(8), 821–835 (2008)
37. Jousset, H., Frieden, M., Demaurex, N.: Stim knockdown reveals that store-operated Ca^{2+} channels located close to sarco/endoplasmic Ca^{2+} ATPases (SERCA) pumps silently refill the endoplasmic reticulum. J. Biol. Chem. **282**(15), 11456–11464 (2007)
38. Croft, W., Reusch, K., Tilunaite, A., Russell, N.A., Thul, R., Bellamy, T.C.: Probabilistic encoding of stimulus strength in astrocyte global calcium signals. Glia **64**(4), 537–552 (2016)
39. Berridge, M.J., Galione, A.: Cytosolic calcium oscillators. FASEB J. **2**(15), 3074–3082 (1988)
40. Zhao, Z., Bing, J., Gu, H.: Bifurcations and enhancement of neuronal firing induced by negative feedback. Nonlinear Dyn. **86**(3), 1–12 (2016)
41. Feudel, U., Neiman, A., Pei, X., Wojtenek, W., Braun, H., Huber, M., Moss, F.: Homoclinic bifurcation in a Hodgkin–Huxley model of thermally sensitive neurons. Chaos **10**(1), 231–239 (2000)
42. Mandelblat, Y., Etzion, Y., Grossman, Y., Golomb, D.: Period doubling of calcium spike firing in a model of a Purkinje cell dendrite. J. Comput. Neurosci. **11**(1), 43–62 (2001)